

## ELECTRONIC SUPPLEMENTARY INFORMATION

### Nitrogen Matters:

### The Difference Between PANH and PAH Formation

Jordy Bouwman,<sup>1,\*</sup> Andras Bodi,<sup>2</sup> and Patrick Hemberger<sup>2</sup>

<sup>1</sup> Sackler Laboratory for Astrophysics, Leiden Observatory, Leiden University, P.O. Box 9513, NL 2300 RA Leiden, The Netherlands

<sup>2</sup> Laboratory for Synchrotron Radiation and Femtochemistry, Paul Scherrer Institute, 5232 Villigen, Switzerland

e-mail: [bouwman@strw.leidenuniv.nl](mailto:bouwman@strw.leidenuniv.nl)

# 1 Acrylonitrile pyrolysis

Acrylonitrile was seeded in argon, pyrolyzed, and mass spectra have been recorded to identify its decomposition products at 9, 10 and 10.5 eV, and at temperatures ranging from room temperature to 1200 K. Mass spectra recorded at the pyrolysis temperature of 1167 K are shown in Figure S1. Peaks at  $m/z$  17, 58, 112 and 126 are also present in the spectrum of unpyrolyzed acrylonitrile and are thus attributed to contaminations in the vacuum chamber or in the sample.

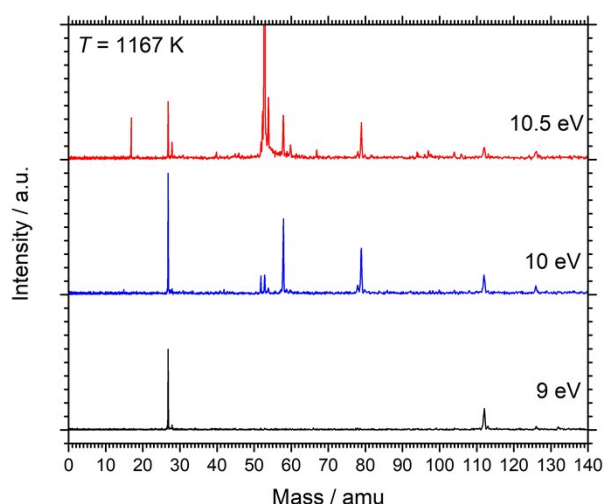


Figure S1: Mass spectra of the products formed from the pyrolysis of acrylonitrile 1167 K and ionized at 9, 10, and 10.5 eV.

The species at  $m/z$  27, 28, 52, and 79 are formed upon pyrolysis of acrylonitrile, which itself is detected at  $m/z$  53 in the spectrum recorded at 10.5 eV. The signal at  $m/z$  27 is ascribed to the vinyl radical that forms in the thermal decomposition of acrylonitrile:



The signal at  $m/z$  27 could also be caused by HCN, but the photon energy applied here is not sufficient to ionize this species with an ionization potential of 13.6 eV.<sup>1</sup>

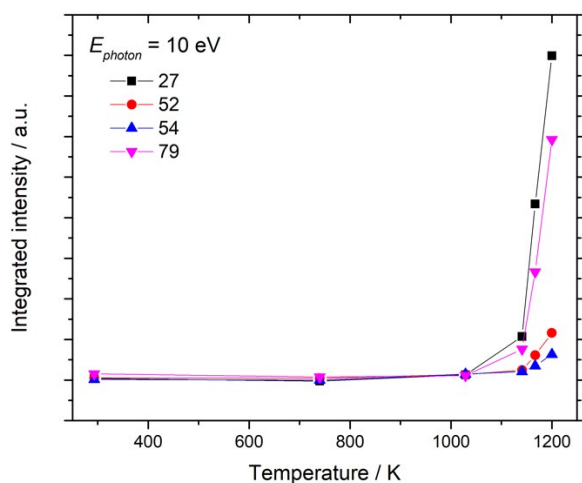


Figure S2: Integrated ion signal of the main product peaks in the pyrolysis of acrylonitrile at a photon energy of 10 eV.

The temperature evolution of the integrated signals of the main products detected at 10 eV is shown in Figure S2. This low photon energy is chosen to suppress dissociative ionization of the precursor. The thermal decomposition of  $C_3H_3N$  sets in at a temperature of 1100 K. Hence, products detected in the pyrolyzed mixture of acrylonitrile and nitrosobenzene are likely formed from the phenyl+acrylonitrile reaction, rather than in the pyrolysis of acrylonitrile.

The weak signal observed in the mass spectrum at  $m/z$  28 at 10.5 eV photon energy is attributed to ethene that forms via hydrogen abstraction by vinyl:



This also explains the detection of a weak signal at  $m/z$  52 ( $C_3H_2N\cdot$ ). The product at  $m/z$  79 is formed via an addition elimination reaction involving the vinyl radical:



## 2 Side products in acrylonitrile + nitrosobenzene pyrolysis

The mass spectrum of the mixture of acrylonitrile and nitrosobenzene in argon is shown in Figure S3. Products that result from the reaction between the phenyl radical and acrylonitrile are described in the main text of the manuscript. Here we discuss the products formed via side reactions. In addition to acrylonitrile pyrolysis, that of 2.5% nitrosobenzene in Ar has also been studied to establish the origin of the minor products.

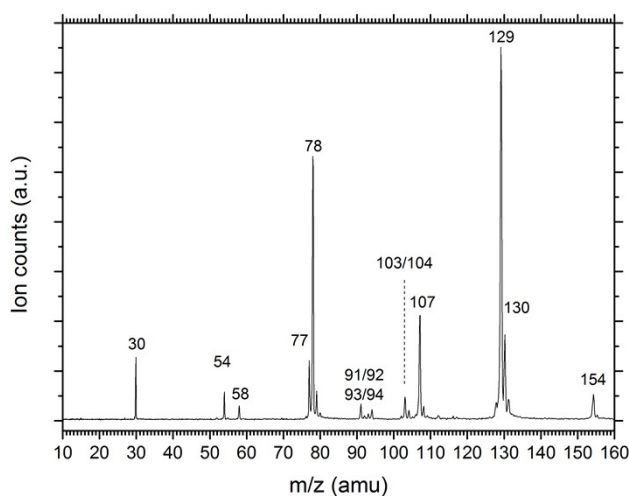


Figure S3: All-electron time of flight mass spectra of a sample containing 2.5% nitrosobenzene and 20% acrylonitrile in argon recorded at a photon energy of 10 eV and at pyrolysis reactor temperature of 690 K.

First, a peak is observed at  $m/z$  30 and is attributed to NO formed upon nitrosobenzene pyrolysis. Another feature is seen at  $m/z$  54 and its ms-TPE spectrum is shown in Figure S4. The ms-TPE spectrum matches well with a simulate spectrum of the 1-cyanoethyl radical that is formed via:



The peak at  $m/z$  58 is attributed to acetone, a contamination in the detection chamber, which does not interfere with the studied chemistry. The cluster of minor species located at  $m/z$  91, 92, 93 and 94 is also apparent in the mass spectra recorded for the pyrolysis of 2.5% nitrosobenzene in Ar and is thus ruled out as products of the phenyl+acrylonitrile reaction. Because of the vanishingly small signal intensity, we do not attempt to assign these peaks.

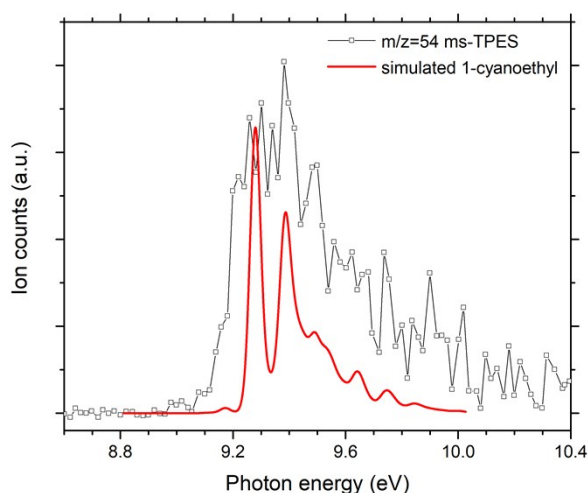


Figure S4: Threshold photoelectron spectrum of the  $m/z$  54 product formed in the pyrolysis of a mixture of nitrosobenzene and acrylonitrile in argon plotted with a simulated spectrum of the 1-cyanoethyl radical.

The peaks observed at  $m/z$  77 and 78 are also detected in the spectra of 2.5% nitrosobenzene in argon, *i.e.*, without acrylonitrile. The  $m/z$  77 species corresponds to the phenyl radical formed as the main product of the thermal decomposition of the precursor. The phenyl radical reacts to form the product observed at  $m/z$  78 and the ms-TPES recorded of that product is shown in Figure S5, which agrees with the photoelectron spectrum of benzene.<sup>2</sup> This product is thus confirmed to be benzene and is most likely formed via hydrogen abstraction by the phenyl radical, via:



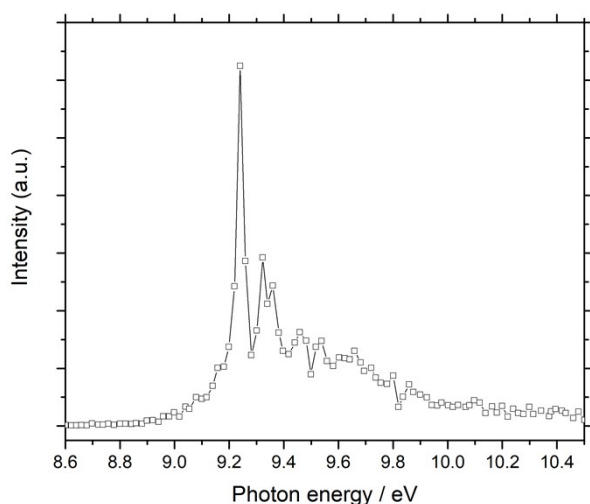


Figure S5: Mass selected threshold photoelectron spectrum of the product formed at  $m/z$  78, benzene.

Small peaks are detected at  $m/z$  103 and 104 and their ms-TPE spectra are shown in Figure S6. These signals are only present in the mass spectra recorded of the pyrolyzed mixture of nitrosobenzene and acrylonitrile and may thus be minor reaction products. The sharp resonance observed at 9.72 eV in the spectrum of the species at  $m/z$  103 matches perfectly with band origin observed in the ionization spectrum of benzonitrile.<sup>3</sup> The ms-TPES of the  $m/z$  104 product shown in Figure S6 displays a sharp onset at 8.4 eV, which coincides with the ionization threshold of styrene.<sup>4</sup>

Benzonitrile formation requires passing a barrier located at 10.1 kJ/mol with respect to the reactants (see below), which makes it an unlikely product of the phenyl + acrylonitrile reaction, in view of the numerous, lower-lying exit channels. However its formation via side reactions cannot be fully excluded. If styrene formation were due to the phenyl + acrylonitrile reaction, on the other hand, it would have to proceed via CN loss from an initial adduct. The computed energy for the styrene +  $\bullet\text{CN}$  product channel is 53.7 kJ/mol. Such high-energy processes can be ruled out, and, hence, we conclude that styrene is formed in a side reaction.

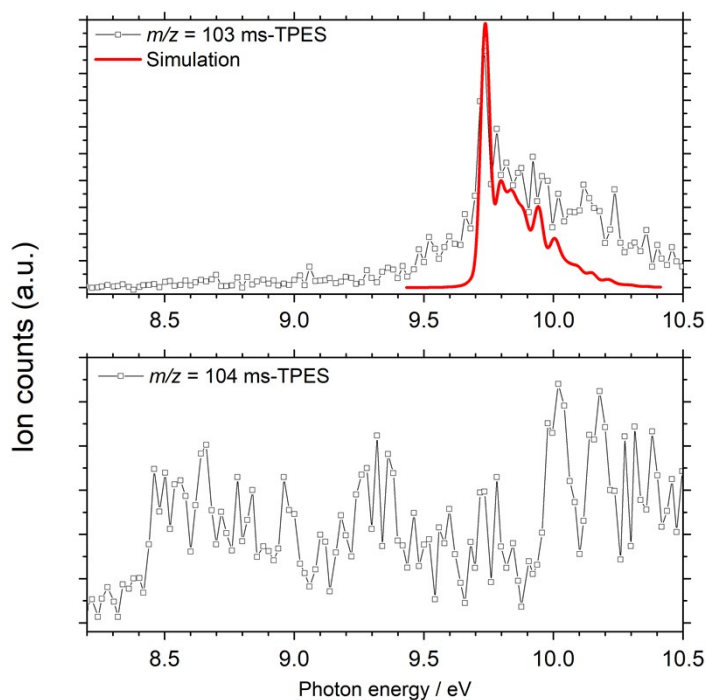
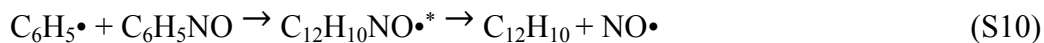


Figure S6: ms-TPE spectra of the products detected at  $m/z$  103 (*top*) shown with the simulated spectrum of benzonitrile (in red) and the ms-TPES of the  $m/z$  104 product (*bottom*), tentatively assigned to styrene.

The ms-TPES of  $m/z$  154 is shown Figure S7. The ionization threshold of this species compares well with the value of 8.2 eV reported for biphenyl in the literature.<sup>5</sup> Biphenyl is possibly formed via the recombination of two phenyl radicals and is collisionally stabilized:



Alternatively, biphenyl can be the product of the phenyl radical reacting with benzene, or nitrosobenzene;



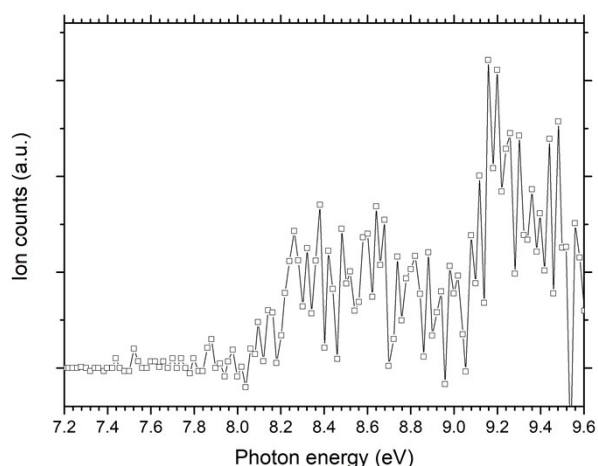


Figure S7: Mass selected threshold photoelectron spectrum of the product formed at  $m/z$  154, assigned to biphenyl.

### 3 Temperature dependence of reaction products

The ms-TPES of the  $m/z$  129 product formed from the phenyl + acrylonitrile reaction was recorded at 630 and 1167 K to check for temperature effects in the product distribution. The spectrum in Figure S8 does not change significantly when the temperature is increased. The only observable effect is the small rise in ion counts around 8.6 eV, which is most likely caused by vibrational hot bands. The unchanged  $m/z$  129 product branching ratios are not unexpected: the transition states to H-loss are submerged and the internal energy of the adduct is predominantly determined its exothermic formation as more than 150 kJ/mol. This can be compared to the less than 40 kJ/mol excess energy available upon heating the system by 500 K.



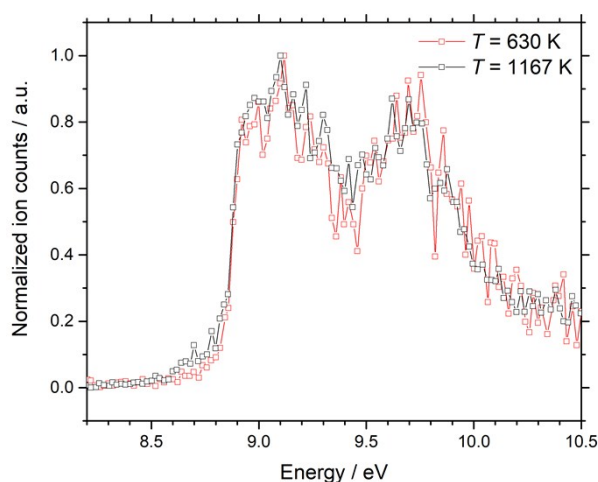


Figure S8: ms-TPES of the  $m/z$  129 product recorded at a pyrolysis temperature of 630 K (red) and 1167 K (black).

## 4 Assignment of main products

### 4.1 $m/z$ 129 product assignment

Out of the 17 isomers considered (see Table S1), CBS-QB3 calculated ionization energies and Franck–Condon simulations carried out at 500 K indicate that seven isomers of  $C_9H_7N$  composition may contribute to the broad band at around 9.1 eV. The experimental spectrum is plotted at the bottom trace along with the simulations of four potential products, namely 2-phenyl acrylonitrile (blue curve), *E*-3-phenylacrylonitrile (red curve), *Z*-3-phenylacrylonitrile (light green curve) and *ortho*-cyanostyrene (dark green), the sum of which reproduces the measured trace very well up to 9.5 eV. The three remaining isomers are excluded, because their formation involves a high-energy transition state, which is unlikely to be overcome in the presence of much lower-lying exit channels. For instance, the formation of meta- and para-cyanostyrene involves additional rearrangement reactions in excess of 20 kJ/mol compared with the entrance barrier of phenyl+acrylonitrile reaction (see Figure S13). Similar thermodynamic and kinetic consideration also apply for the imine species ( $Ph-C(=NH)-C_2H$ ), see PES in Figure S14.

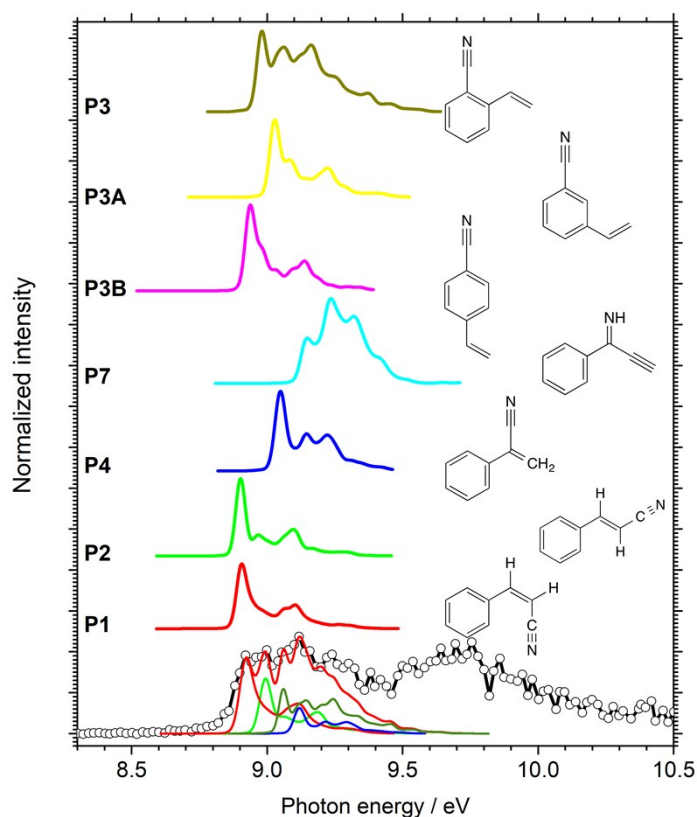


Figure S9: Experimental ms-TPE spectrum of the reaction products at  $m/z$  129 shown together with Franck–Condon simulated spectra of possible isomers. The labels left of the simulated TPE spectra refer to the structure names in the potential energy surfaces. In order to match the calculated and experimental TPE spectra, we fitted the adiabatic ionization energies within a 100 meV confidence range of the CBS-QB3 calculated values.

#### 4.2 $m/z$ 130 product assignment

Figure S10 shows the experimental ms-TPE spectrum of the radical intermediates at  $m/z$  130. Ionization energies calculated at the CBS-QB3 level suggest that seven different isomers may be the carrier of the ms-TPES. In comparison with our calculated reaction pathways and the identified closed shell  $m/z$  129 products, we assign the most prominent features of the TPES to  $\alpha$ -methyl- $\alpha$ -cyano-benzyl radical (dark blue curve), the 2-cyano-1-phenylethyl radical (dark red curve), and the 6-cyano-1-ethenylcyclohexa-2,4-dien-1-yl radical (cyan curve) and these are plotted onto the  $m/z$  130 spectrum.

Four potential radical intermediates can be excluded based on energetics arguments. While the presence of hydrogenated quinoline (see [17] in Figure S17) would be compatible with the measured TPE spectrum, it can only be formed over a barrier at 65.1 kJ/mol and would promptly react further to form quinoline, ruling it out as a contributor. Furthermore, the spectrum of phenyl-amino-propadienyl (shown in green in Figure S10) fits the resonance observed at 7.4 eV, yet this species is calculated to be formed over a barrier of 20.2 kJ/mol with respect to the reactants (see [13] in Figure S14) and is thus not expected to be formed. The two 6-cyano ethenylcyclohexa-2,4-dien-1-yl radicals (shown in blue and red in Figure S10) can also be ruled out, as they would need to be formed over barriers exceeding 20 kJ/mol. (see Figure S13)

As mentioned in the main article, the ionization energies of the direct adducts **AC1–AC3** fall within the range of the observed ms-TPES signal. However, both the change in geometry upon ionization and the associated stabilization are large, which leads to small FC factors and vanishingly small photoelectron signal at threshold. This is not compatible with the dominant peak in the ms-TPES at around 7.5 eV. The calculated vertical ionization energies of **AC1–AC3** (8.6–9 eV, see Table S2) do not correspond to features in the ms-TPES at these energies, although they may be suppressed by the much stronger  $^{13}\text{C}$  contribution of the  $m/z$  129 signal in this energy range. It is therefore unclear whether the direct adducts (**AC1–AC3**) quantitatively lose hydrogen to form the species with  $m/z$  129 before their re-thermalization and stabilization or are only inefficiently ionized.

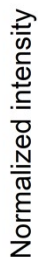


Figure S10: Experimental ms-TPE spectrum of the radical intermediates at  $m/z$  130, shown together with Frack–Condon simulated spectra of radicals that possibly contribute.

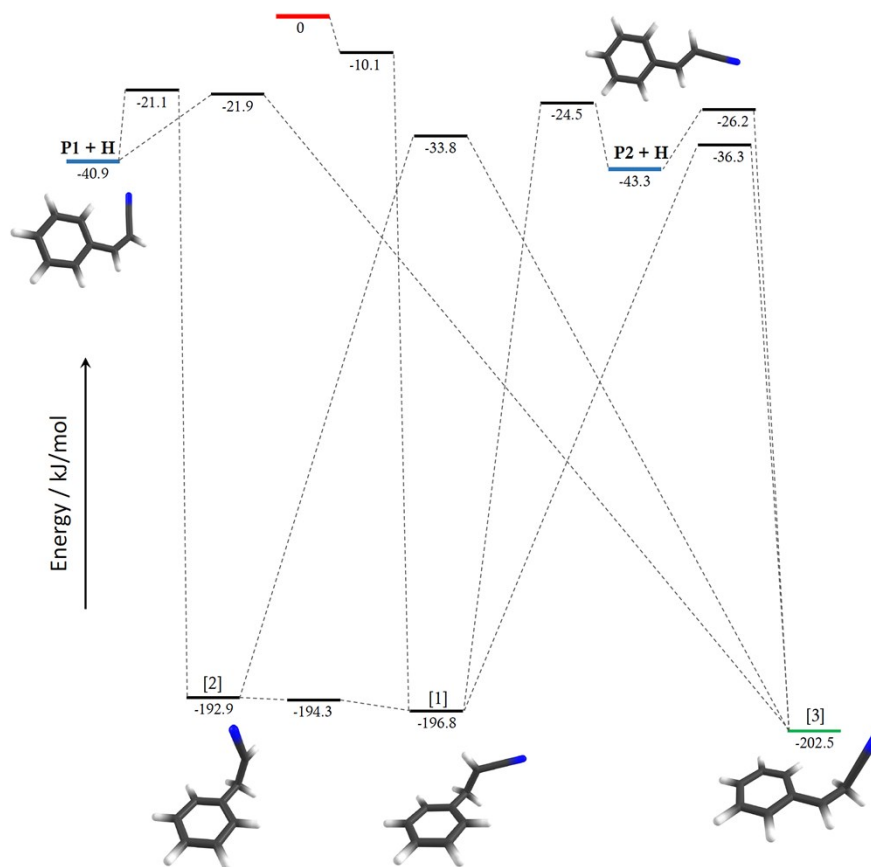


Figure S11: Potential energy surface of the phenyl radical adding to the terminal carbon (C3) on acrylonitrile.

## 5 Detailed description of the potential energy surface

Detailed potential energy surfaces are provided in Figures S11–S14 and the structures of the transition states are displayed in Figures S18–S20. Acrylonitrile can add to the phenyl radical in four different ways. First, we refer to Figure S11 where C3 of acrylonitrile adds to the sigma radical site of phenyl, forming the resonance stabilized radical **[1]** over a submerged barrier at  $-10.1$  kJ/mol. This intermediate can directly lose a hydrogen atom over to form E-3-phenylacrylonitrile (**P2**) or isomerize to **[2]** after which it can form Z-acrylonitrile (**P1**). Alternatively, **[1]** can undergo a hydrogen shift to form **[3]** from where **P2** can again be formed.

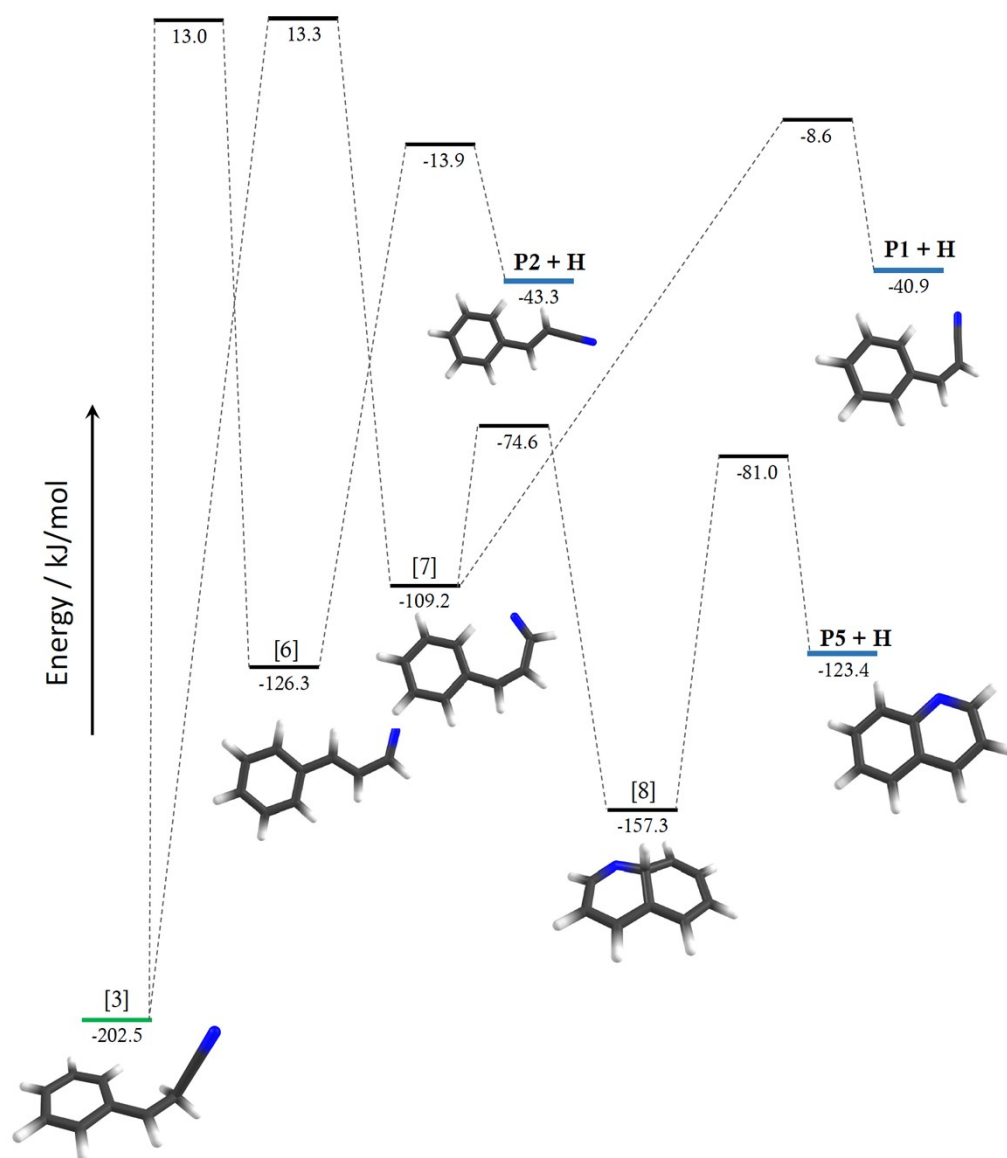


Figure S12: Potential energy surface displaying possible isomerization and product formation mechanisms starting from [3].

A number of isomerization steps are possible starting from [3]. First, as shown in Figure S12, a hydrogen migration over a barrier at 13.0 kJ/mol results in [6], which can lose a hydrogen atom over a barrier at -13.9 kJ/mol to form **P2**. Second, [3] can isomerize via a hydrogen migration that lies slightly higher in energy (13.3 kJ/mol) to form [7]. From here, **P1** can form via hydrogen loss over a barrier at -8.6 kJ/mol, or a hydrogen shift (-74.6 kJ/mol) to form [8] followed by H-loss over a transition state at -81.0 kJ/mol yields quinoline (**P5**).

Alternative isomerization processes are displayed in Figure S13. Ortho-cyanostyrene (**P3**) can be formed from **[3]** via the stationary points **[4]** and **[5]**. Meta-cyanostyrene (**P3A**) can form by hydrogen loss after isomerization from **[5]** to **[18]** and para-cyanostyrene (**P3B**) could form after further isomerization of **[18]** to **[19]**. The rate limiting barriers for the formation of meta- and para-cyanostyrene are respectively 23.2 and 22.3 kJ/mol above the entrance channel of the reaction and are thus not likely to be formed.

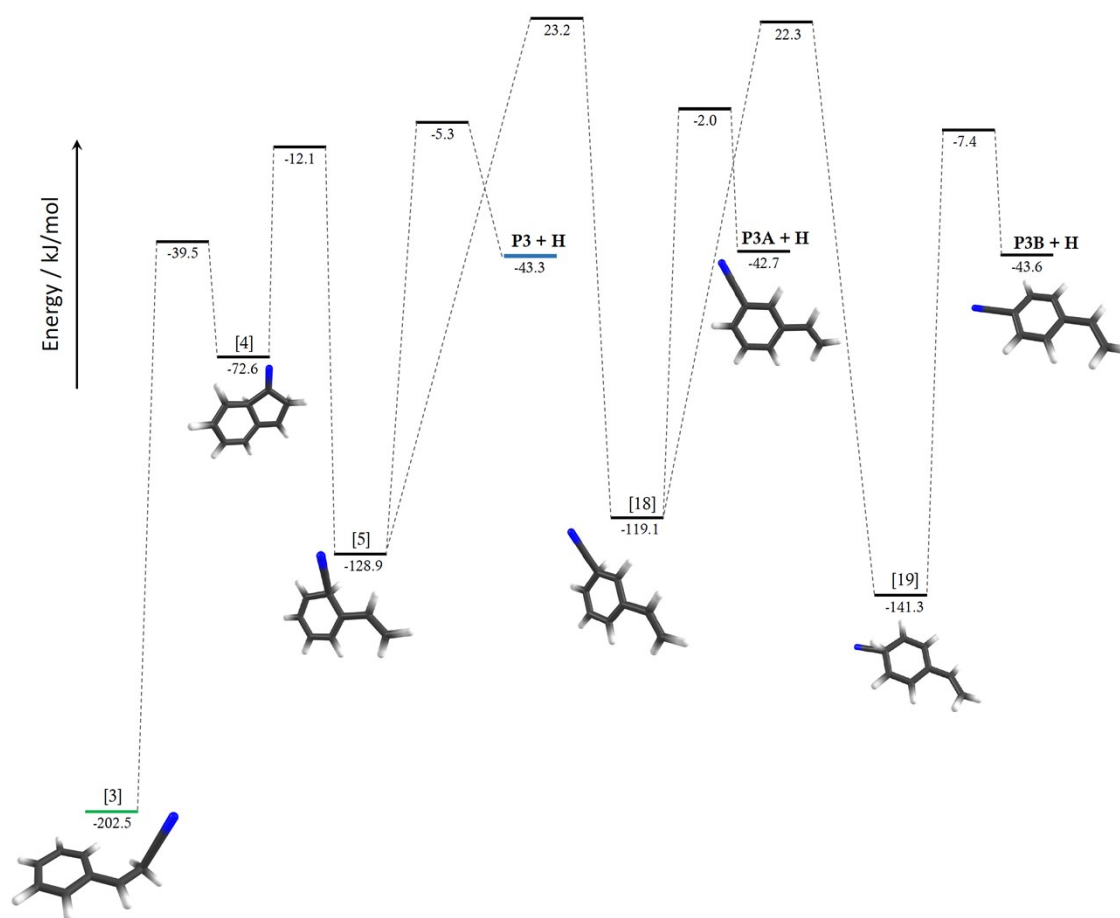


Figure S13: Formation of the various cyano styrenes from starting from **[3]**.

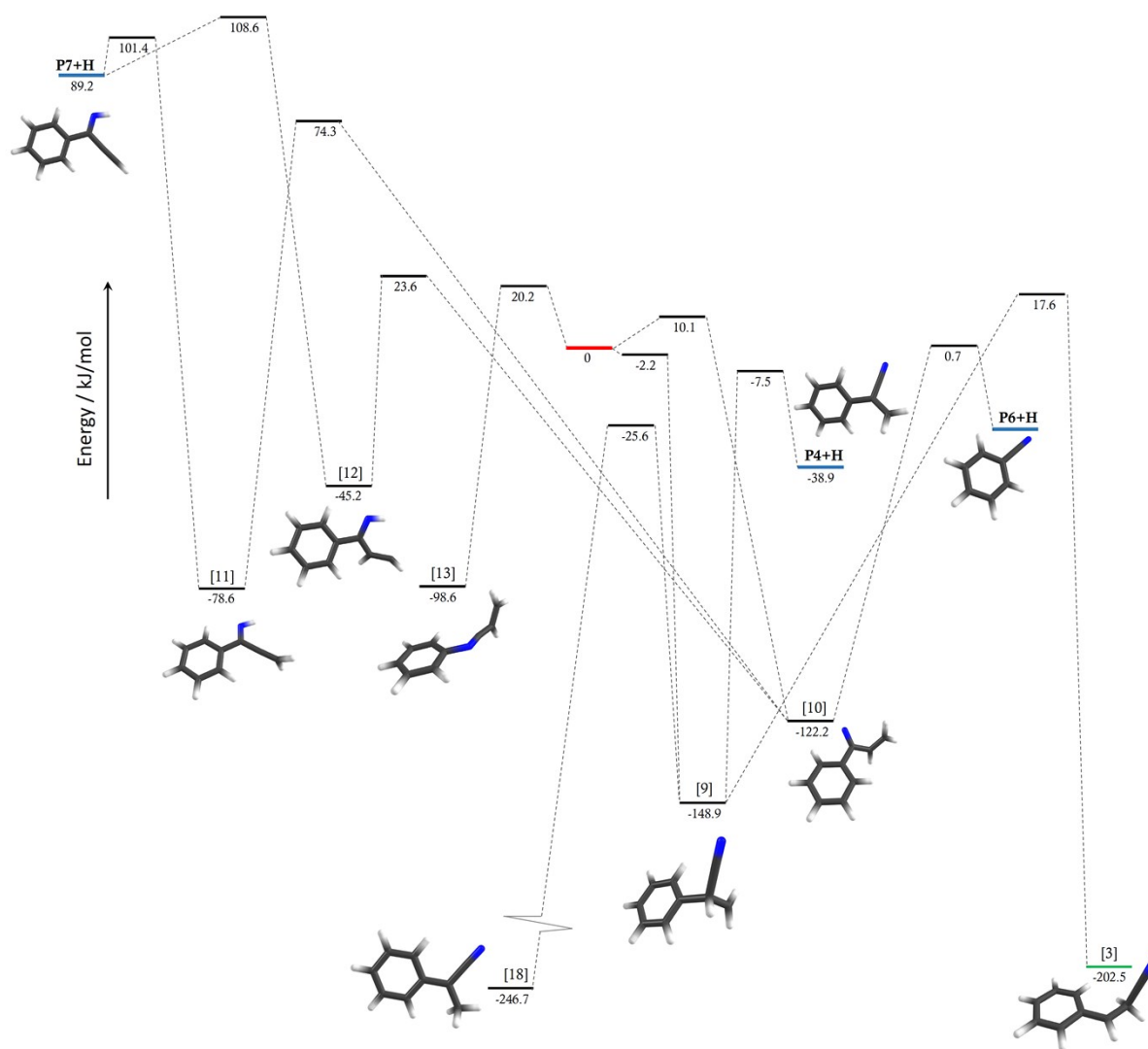


Figure S14: Potential energy surface of the phenyl radical adding to C1, C2 and N of acrylonitrile.

Three more possible additions of acrylonitrile to phenyl are displayed in Figure S14. First, the phenyl radical can add to C2 of acrylonitrile over a submerged barrier at  $-2.2$  kJ/mol, forming **[9]**. From here, a barrier at  $-25.6$  kJ/mol can be crossed to form **[18]**, which is very stable at an energy of  $-246.7$  kJ/mol and is in fact far of the scale presented in Figure S14. Another possible pathway from **[9]** is hydrogen loss over barrier at  $-7.5$  kJ/mol. Stationary point **[3]** can also be reached from **[9]** over a barrier at  $17.6$  kJ/mol and thus connects to the PES shown in. Addition of phenyl to C1 of acrylonitrile atom goes over a barrier at  $10.1$  kJ/mol



and results in [10]. From here, benzonitrile (**P6**) can be formed via vinyl loss over a barrier at 0.7 kJ/mol. Alternatively, hydrogen shifts can occur starting from [10] resulting in the imine intermediates [11] and [12] over a barrier at 74.3 or 23.6 kJ/mol, respectively. From here, 1-phenylprop-2-yn-1-imine (**P7**) can be formed from these stationary point via hydrogen loss over a barrier at 108.6 or 101.4 kJ/mol from [12] and [11], respectively. However, the formation of these species is very unlikely, given the energies involved in their formation. Addition of the phenyl radical to the nitrogen on acrylonitrile is accompanied by a barrier of 20.2 kJ/mol and results in [13]. All pathways from here are found to be far too energetic to be competing.

### 5.1 RRKM model for the **AC1** adduct

We can calculate *ab initio* dissociation and unimolecular reaction rates as a function of internal energy, based on the *ab initio* energetics as well as minimum densities of states and transition state numbers of states. The state functions in the RRKM equation are calculated from harmonic vibrational frequencies:

$$k(E) = \frac{\sigma N^{\ddagger}(E - E_0)}{h\rho(E)} \quad . \quad (S11)$$

In (S11),  $\sigma$  represents the symmetry number of the fragmentation channel (set to 1 in our case),  $h$  is Planck's constant,  $N^{\ddagger}(E - E_0)$  is the number of internal states for the transition state at internal energy  $(E - E_0)$ , and  $\rho(E)$  is the density of states for the precursor at internal energy  $(E)$ . The number of states of the transition state for the reverse, dissociation reaction was approximated based on the harmonic frequencies evaluated at an arbitrary, 2.2 Å C–C bond length between acrylonitrile and the phenyl radical. The resulting adduct lifetime and branching ratios are presented in Figure S15. At the experimental temperature, corresponding to about 50 kJ/mol internal energy, the total statistical life time of **AC1** is on the order of 10 μs. The back reaction is always a minor channel, and **AC1** is modeled to form **P2** and **P1** predominantly. At

lower temperatures, the lifetime may be high enough to allow for rethermalization, which would effectively stop the reaction before H elimination. The relative reaction rates to quinoline (**P5**), mirrors the high barrier found in the PES (Figure 4) and the branching ratio does not exceed 1% even at 400 kJ/mol internal energy.

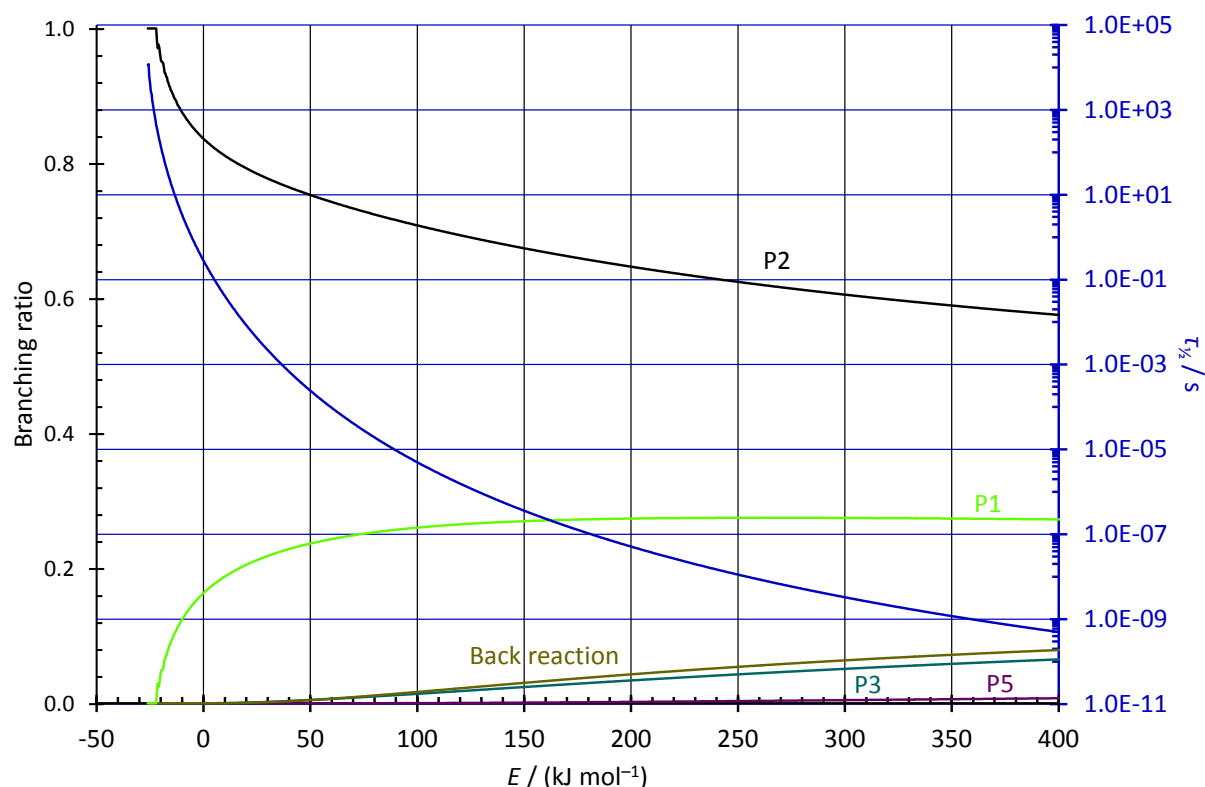


Figure S15: Ab initio RRKM prediction of the lifetime and product branching ratios of **AC1**, considering the highest-lying rate determining transition states to **P1**, **P2**, **P3**, **P5** (quinoline), and the back reaction

## 5.2 Differences between quinoline and naphthalene formation

To compare the unproductive phenyl+acrylonitrile reaction yielding quinoline with the productive and isolectronic phenyl+vinylacetylene path yielding naphthalene, we also calculated the analogous reaction energy curves for the lowest energy paths in both systems for

quinoline and naphthalene, as shown in Figures S16, S17 and S18. The transition states are available in Figures S19, S21 and S23.

First, we explored the  $C_{10}H_9$  potential energy surface to find a pathway to naphthalene that is analogous to our lowest energy pathway to quinoline (Figure S16). The formation of both naphthalene and quinoline is kinetically hindered by barriers above the entrance channel of the reaction via this mechanism. The initial steps of the two mechanisms are very similar in terms of the energies of the transition states and intermediates involved. However, major differences start to show when [7] and [N11] are formed for quinoline and naphthalene, respectively. The  $C_{10}H_9$  structure exhibits a larger drop in energy than the N-containing species and this effect becomes more pronounced when the second ring is closed, emphasizing the difference in fully aromatic species compared to nitrogen bearing ones.

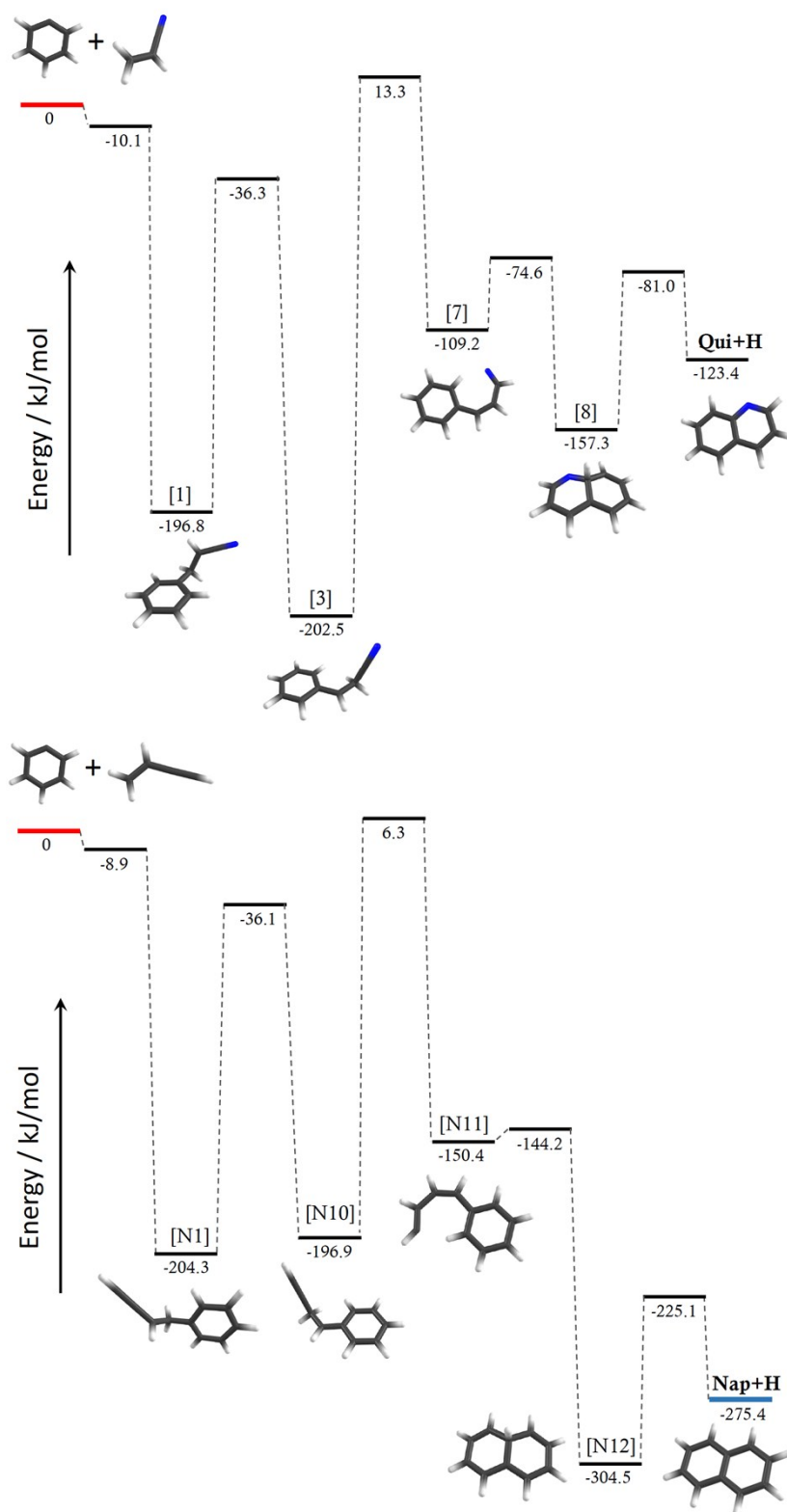


Figure S16: A detailed comparison of the lowest energy pathway to quinoline reported here with the analogous pathway leading to naphthalene.

The second pathway we investigated is shown in Figure S17. Here we compare the lowest energy mechanism to naphthalene reported by Parker et al.<sup>6</sup> replicated at the CBS-QB3 level with the analogous pathway to quinoline (top). This figure reproduces Figure 6 of the main text, where its detailed discussion is also presented. In short, ring closure, hence the partial saturation of the C≡N or C≡CH group is quite different, and the stabilization gained in the latter case results in a downhill naphthalene formation pathway without an overall barrier. The stability of the nitrile group results in a large ring closure activation energy, which kinetically hinders the process in the case of quinoline formation.

Lastly, for completeness, we also replicated the second barrierless pathway to naphthalene reported by Parker et al.<sup>6</sup> The pathway is shown in Figure S18 and, besides the slight differences in energy compared to the PES published by Parker et al.,<sup>6</sup> we find a fairly high lying transition state at  $-5.1$  kJ/mol connecting [N8] and [N9] which was not identified previously and renders this channel much less important in the formation of naphthalene. An analogous pathway to quinoline has not been identified, as addition of the nitrogen atom of acrylonitrile to the phenyl radical site is energetically very unfavorable (see Figure S14).

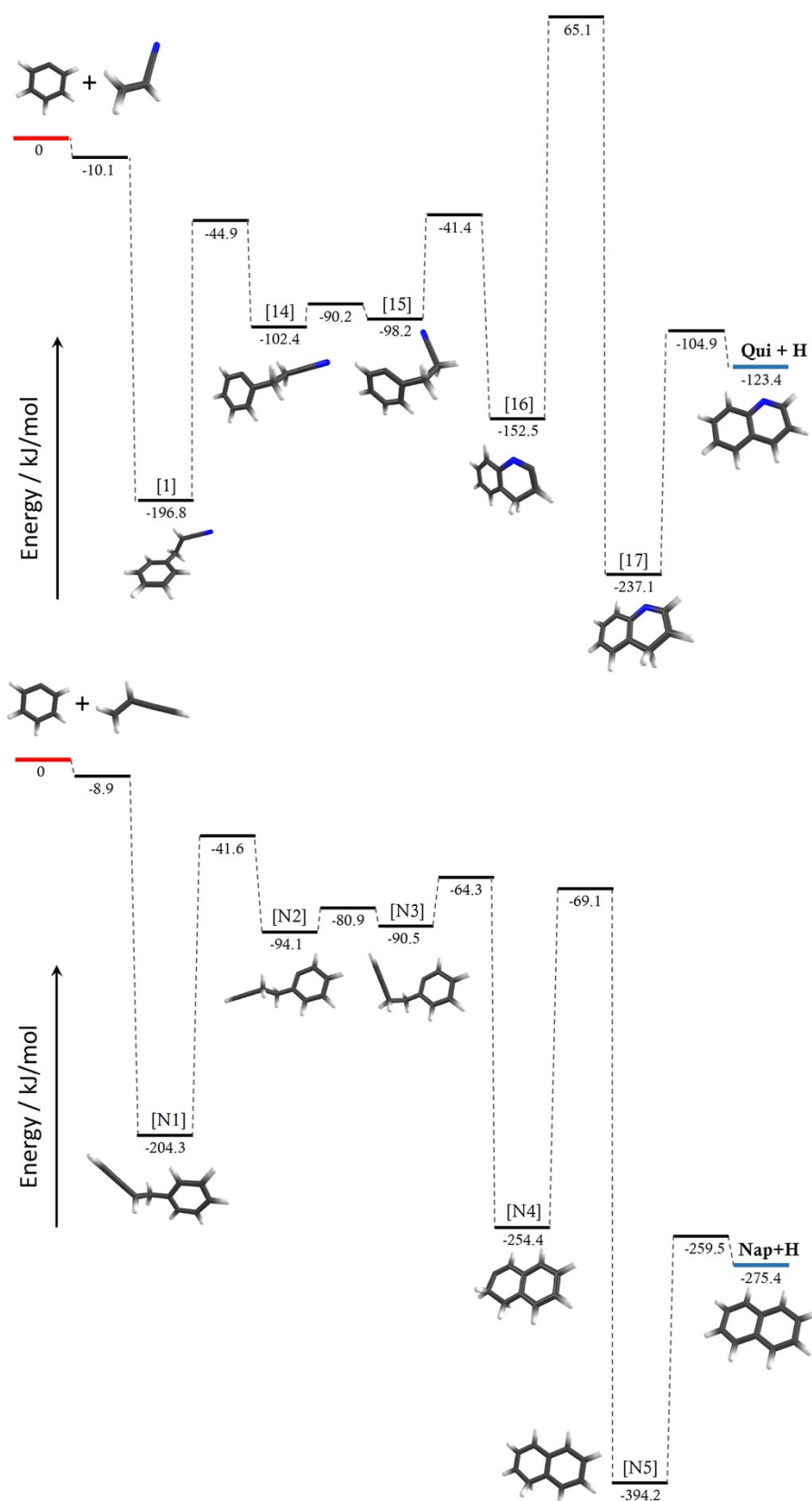


Figure S17: Alternative channel leading to quinoline (top) together with the analogous formation of naphthalene from the phenyl + vinylacetylene reaction (bottom).

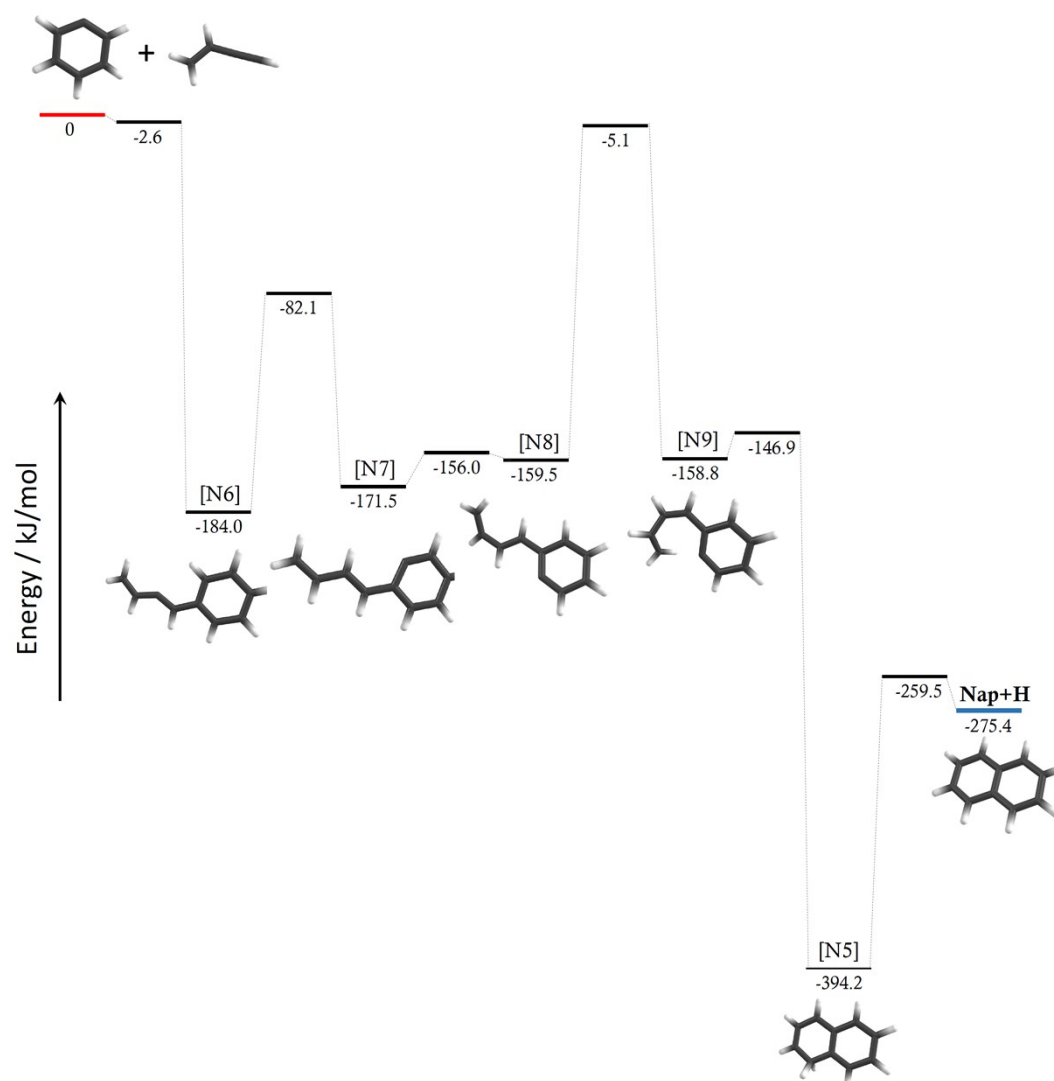


Figure S18: An alternative pathway to naphthalene starting from phenyl + vinylacetylene. All energies are relative to the entrance channel.

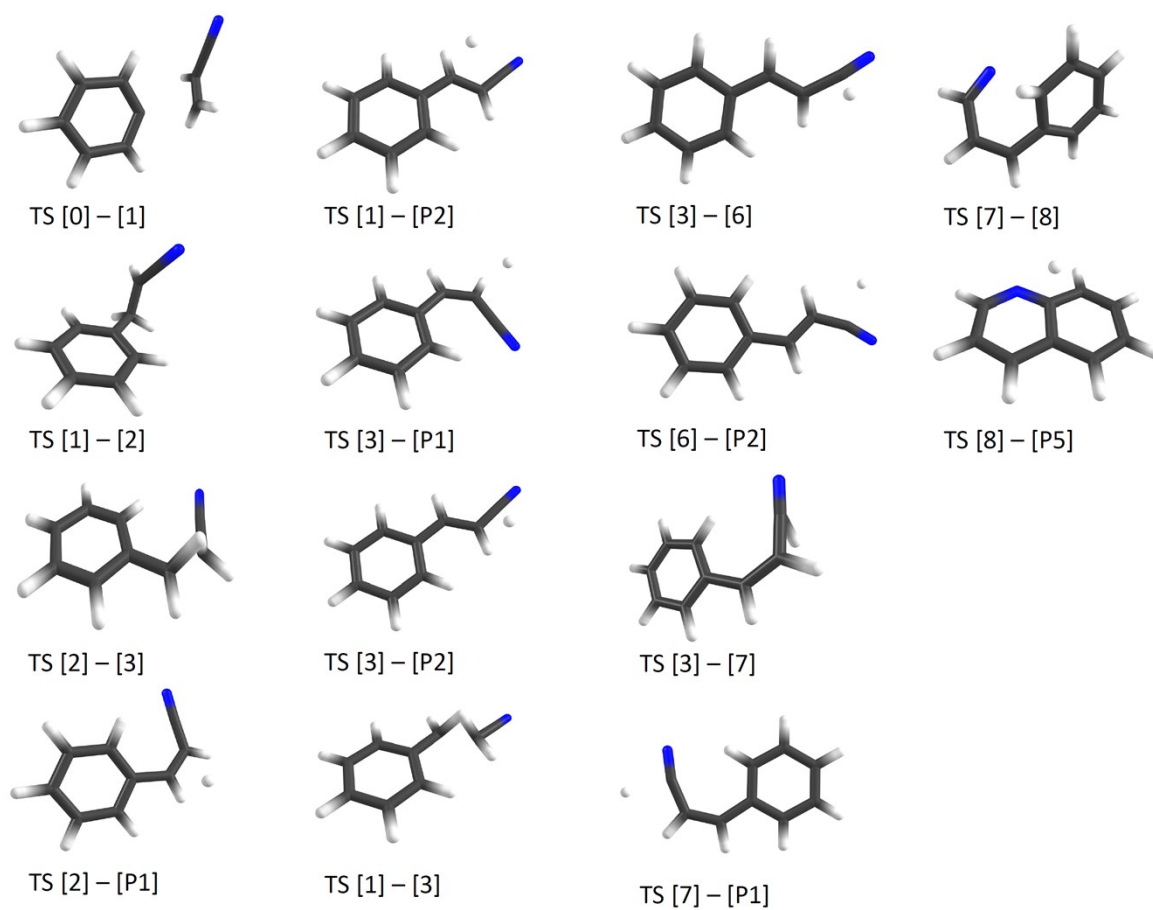


Figure S19: Transition states belonging to Figures S11 & S12.

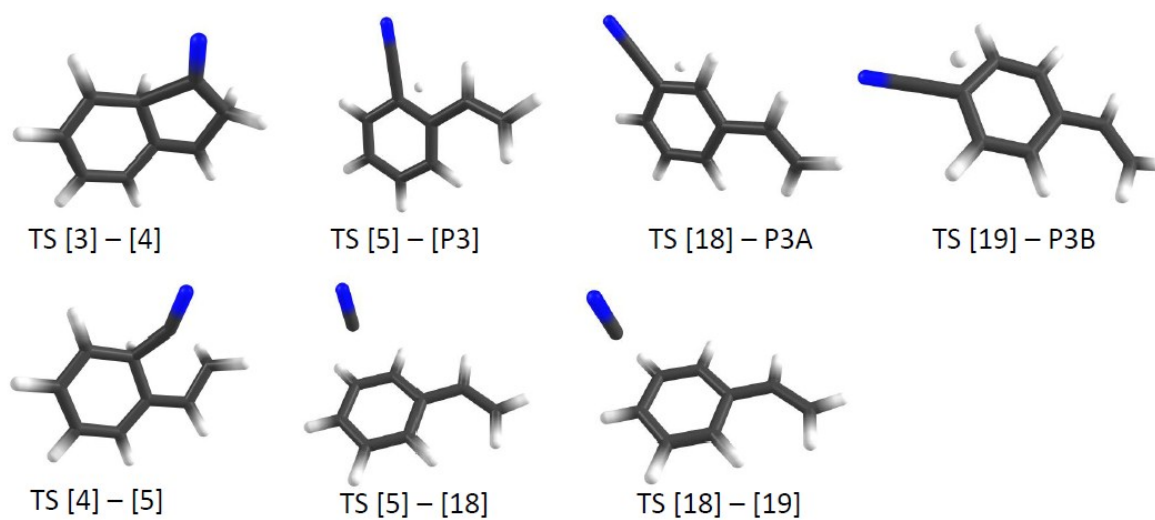


Figure S20: Transition states belonging to Figure S13



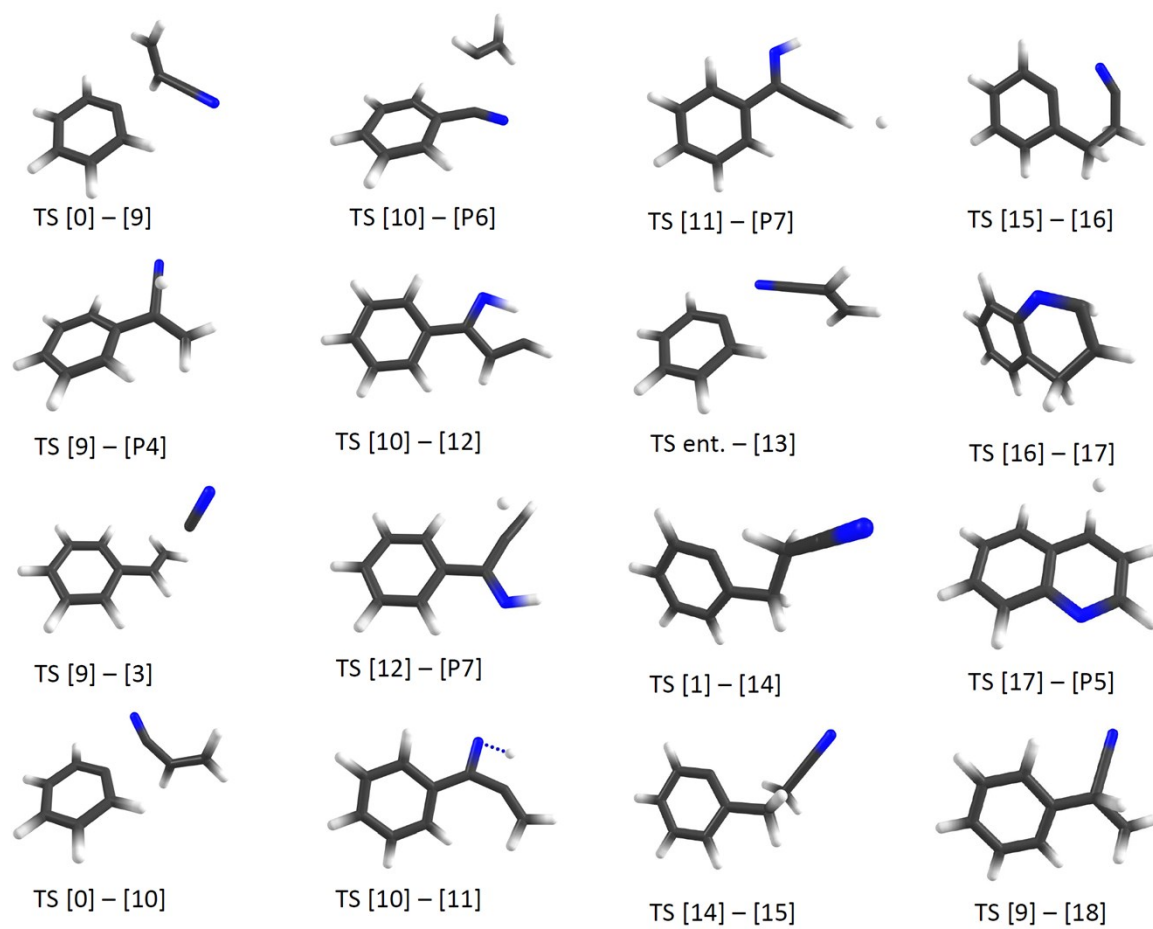


Figure S21: Transition states belonging to Figures S14 & S15.

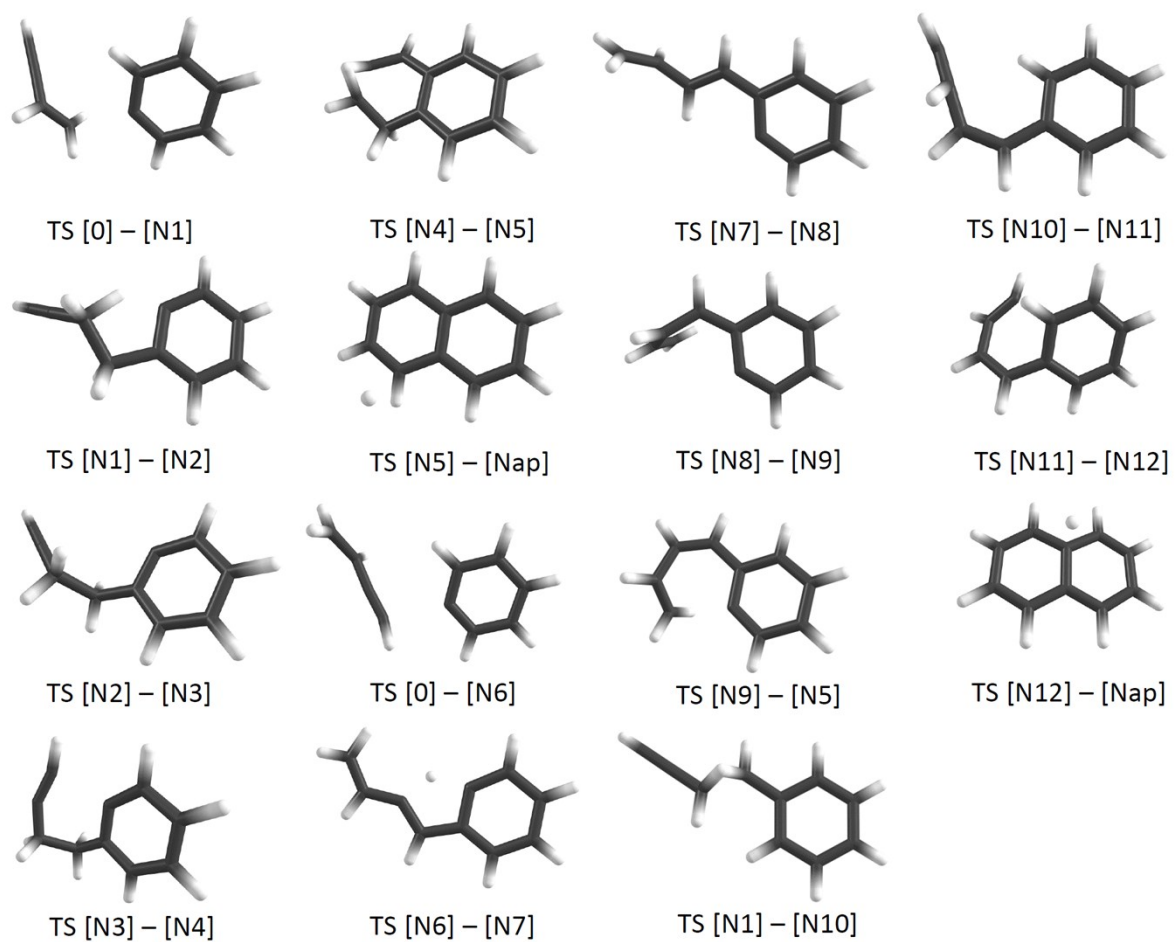
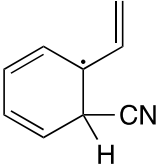
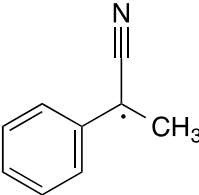
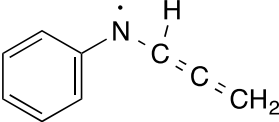
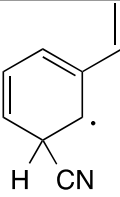
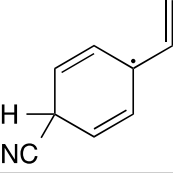
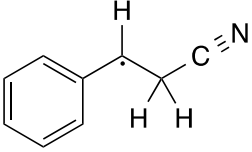
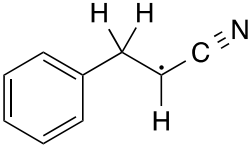
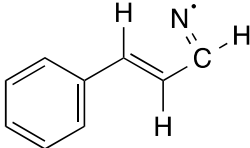
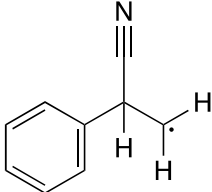
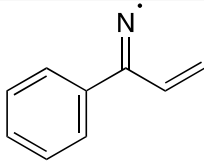
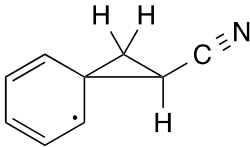
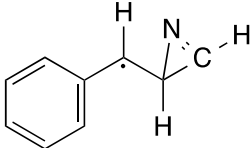
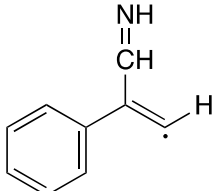
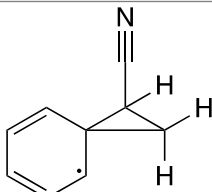
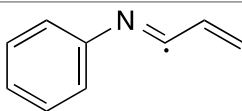
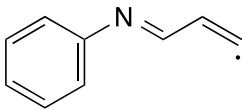
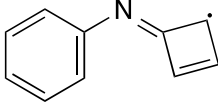
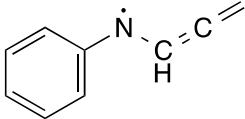
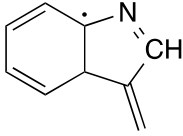
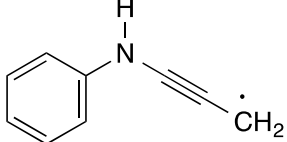
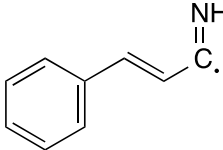
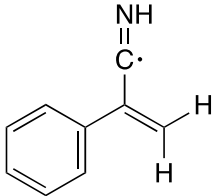
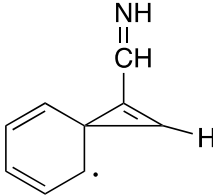
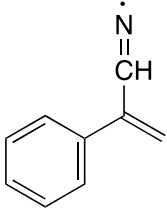
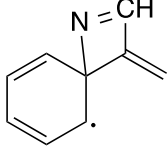
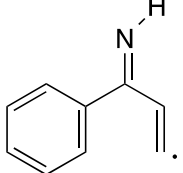
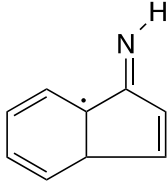


Figure S22: Transition states belonging to Figures S16, S17 and S18.

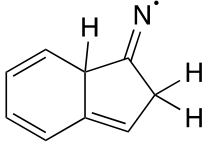
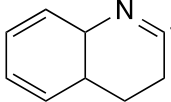
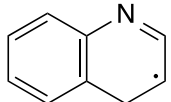
**Table S1. Possible contributors to the  $m/z = 130$  signal of  $C_9H_8N$  composition.**

isomer	AIE calc. in eV			VIE calc. in eV	relative energy to entrance channel in kJ/mol
	AIE exp. /eV	DFT	CBS-QB3	DFT	
 [C]	7.38		7.371		-128.5
 [A]	7.64	7.552	7.698	7.645	-246.6
 [B]		7.178	7.414		-75.8
 [C]			7.593		-118.7
 [B]			7.416		-140.8
 [B]	ca. 7.5	7.344	7.435	7.419	-202.5
 [AC1]		7.761	7.677	8.611	-196.9

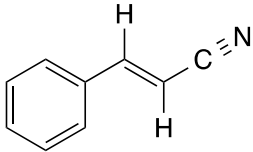
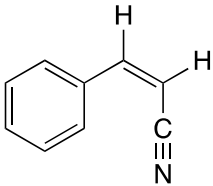
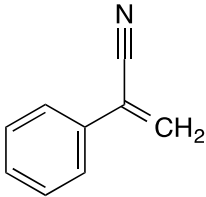
	7.616	7.629	9.138	-126.4
	7.178	7.181	8.521	-149.1
[AC2]				
	7.512	7.491	8.942	-122.2
[AC3]				
	6.767	6.859		-118.0
	6.647	6.818		-48.1
	7.250	7.293	8.749	-40.9
	6.767	6.859		-118.0
	5.856	5.726		-98.7
[AC4]				
	7.027	6.706		-15.2
	6.405	6.745		-19.1

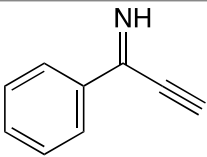
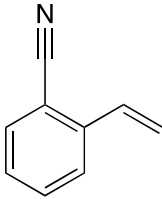
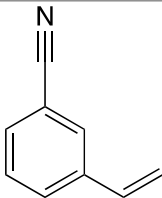
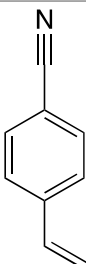
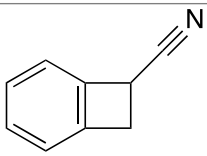
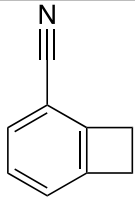
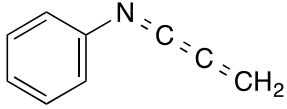
	6.339	6.203	-67.9
	6.698	6.908	-135.8
	6.373	6.381	-54.5
	6.226	6.223	-138.6
	6.289	6.097	-116.2
	6.261	6.340	51.1
	8.363	8.354	-133.9
	6.942	7.100	-12.9
	6.137	6.186	-47.1
	6.901	7.107	-136.0

	7.877	7.831	-78.6
	5.374	5.524	11.7
	6.132	6.112	-45.0
	5.650	5.683	-13.9
	5.920	5.948	-100.4
	8.097	8.203	-78.7
	6.883	7.149	-84.9
	4.967	4.932	-16.9
		6.900	-157.3
		6.785	-154.8

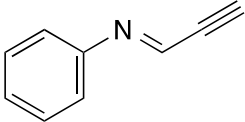
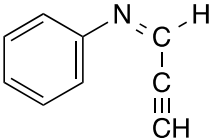
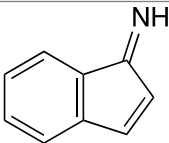
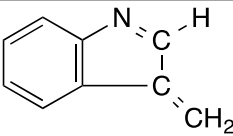
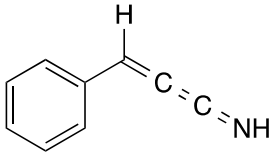
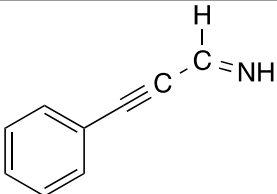
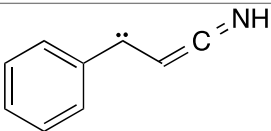
	6.085	-72.3
	6.957	-145.2
	7.409	-237.1

**Table S2. Possible contributors to the  $m/z = 129$  signal of  $C_9H_7N$  composition.**

isomer	AIE calc. / eV		AIE /eV	rel. energy to [entrance channel -H] in kJ/mol
	DFT	CBS-QB3	exp.	
 <b>[P2]</b>	8.583	8.905	9.00	-43.2
 <b>[P1]</b>	8.587	8.903	8.92	-40.9
 <b>[P4]</b>	8.686	9.035	9.12	-38.8

	8.732	9.134	99.7	
	8.633	8.980	9.06	-43.4
<b>[P3]</b>				
	8.672	9.027	-42.5	
	8.598	8.937	-43.4	
	8.983	9.291	13.9	
	9.014	9.328	5.2	
	7.434	7.723	138.5	



	7.912	8.187	120.2
	7.836	8.139	123.6
	8.190	8.475	-48.8
	8.268	8.574	-39.0
	7.802	8.105	109.8
	8.325	8.645	94.0
	6.311	6.538	261.7

## References

1. C. Baker and D. W. Turner, *Proceedings of the Royal Society of London. Series A. Mathematical and Physical Sciences*, 1968, **308**, 19-37.
2. G. I. Nemeth, H. L. Selzle and E. W. Schlag, *Chem. Phys. Lett.*, 1993, **215**, 151-155.
3. C. H. Kwon, H. L. Kim and M. S. Kim, *J. Phys. Chem. A*, 2003, **107**, 10969-10975.
4. M. J. S. Dewar and S. D. Worley, *J. Chem. Phys.*, 1969, **50**, 654-667.
5. J. H. D. Eland and C. J. Danby, *Z. Naturforsch. A*, 1968, **23**, 355.
6. D. S. N. Parker, F. T. Zhang, Y. S. Kim, R. I. Kaiser, A. Landera, V. V. Kislov, A. M. Mebel and A. G. G. M. Tielens, *Proc. Natl. Acad. Sci.*, 2012, **109**, 53-58.
7. L. Zhao, R. I. Kaiser, B. Xu, U. Ablikim, M. Ahmed, M. V. Zagidullin, V. N. Azyazov, A. H. Howlader, S. F. Wnuk and A. M. Mebel, *The Journal of Physical Chemistry Letters*, 2018, **9**, 2620-2626.